Journal of Materials and Construction
ISSN 2734-9438
Website: www. jomc.vn

Influence of curing methods on the compressive strength development of 3D-printed concrete unit cells

Pham Thi Loan[1*], Nguyen Thi Hoai Thu[1]

[1]Faculty of Engineering and Technology, Haiphong University

KEYWORDS

3D Concrete Printing
Curing Methods
Natural air-drying
Membrane sealing
Water Immersion
Compressive Strength
Relative Performance

ABSTRACT

This study provides a direct, quantitative comparison of three practical curing methods—Natural air-drying (ND), Membrane sealing (MB), and Water Immersion (WI)—on the compressive strength development of 3D-printed concrete (3DPC). Unit cell specimens were fabricated and subjected to the curing regimes immediately after printing, with strength evaluated at 7 and 28 days. Results demonstrate a substantial influence of the curing method. Membrane sealing (MB) proved most effective, yielding the highest strength (16.7 MPa and 19.7 MPa at 7 and 28 days, respectively). Using MB as a baseline (100%), a Relative Performance Index (RPI) revealed that Immersion (WI) and Natural curing (ND) retained only 89% and 80% of the 28-day strength, respectively. Qualitative analysis of failure modes showed cohesive vertical cracking without interlayer delamination, indicating that interlayer bonds remained competent and that the strength reduction under poor curing is primarily due to a generalized weakening of the cementitious matrix. This finding underscores that effective curing enhances overall material homogeneity. The pronounced performance deficit, particularly under natural drying, directly quantifies the critical vulnerability of 3DPC's layered microstructure to moisture loss. The findings deliver clear, data-driven evidence for implementing impermeable membrane curing as a vital and practical site practice to ensure the mechanical performance of digitally fabricated concrete.

1. Introduction

The architecture, engineering, and construction industry is undergoing a digital transformation, with additive manufacturing, commonly known as 3D Concrete Printing (3DPC), positioned at its forefront [1], [2], [3], [4]. This technology transcends conventional formwork-based practices, enabling the automated, layer-by-layer deposition of cementitious materials to create complex, customized geometries. The potential benefits are substantial, including unprecedented design freedom, significant reductions in material waste through near-net-shape fabrication, decreased reliance on manual labor, and the potential for improved construction efficiency [5] [6] [1], [7], [8]. Consequently, 3DPC is rapidly evolving from a laboratory-scale novelty to a viable solution for constructing both architectural components and load-bearing structural elements.

However, this transition from prototype to reliable structural system is contingent upon overcoming fundamental materials science challenges inherent to the process. Unlike monolithic cast concrete, which consolidates into a relatively homogeneous and isotropic matrix, the extrusion-based deposition in 3DPC results in a distinctly anisotropic and layered microstructure [9], [10], [10], [11]. In this system, the macroscopic mechanical performance is not governed by the bulk material properties alone but is critically mediated by the quality of the interfacial transition zones (ITZs) between successively deposited filaments [12], [13], [13], [14] [13] [13]. These interfaces, akin to "cold joints," are microstructurally vulnerable, often exhibiting higher porosity and weaker bonding, making them the potential weak link in the printed structure [15].

This anisotropic nature intertwines with a second critical vulnerability: extreme sensitivity to early-age moisture conditions [16]. The printing process creates an element with an exceptionally high surface-area-to-volume ratio, providing a vast pathway for rapid moisture evaporation [17], [18]. This desiccation is particularly detrimental at the interlayer regions, where sufficient moisture is essential for continued hydration and the development of strong chemical and mechanical bonds between layers. Inadequate moisture retention can thus severely inhibit strength gain, exacerbate anisotropic behavior, and promote premature cracking or delamination failures.

Therefore, post-printing curing the process of maintaining adequate moisture and temperature is not a mere procedural afterthought in 3DPC; it is a fundamental technological prerequisite for achieving designed mechanical performance and ensuring structural integrity. While the principles of hydration are universal, the optimal curing strategy for 3DPC may differ markedly from established protocols for conventional concrete. Standards and guidelines for cast-in-place concrete [19], [20] are prescriptive and well-established, yet they are not tailored to address the unique microstructural configuration and moisture loss dynamics of printed elements.

*Corresponding author: loanpt80@dhhp.edu.vn

Received 15/01/2026, revised 25/03/2026, accepted 27/03/2026
Link DOI: https://doi.org/10.54772/jomc.v16i01.1226

A review of the extant literature reveals a significant research gap. While substantial effort has been dedicated to developing printable materials, optimizing rheology, and characterizing mechanical properties under idealized, laboratory curing conditions (e.g., constant water immersion or high-humidity chambers). There is a pronounced scarcity of studies systematically investigating the efficacy of practical, on-site, applicable curing methods. Nodehi et al. [21] provided a comprehensive review on the effect of supplementary cementitious materials on 3D printed concrete, noting that curing regime significantly influences the performance of mixtures containing fly ash and other SCMs. Chen et al. [22] experimentally examined the effect of curing methods applied during printing intervals on interlayer bonding strength, highlighting the critical role of moisture retention in the vulnerable interfacial zones. More recently, the influence of temperature and humidity on the mechanical properties of 3D-printed concrete was systematically evaluated, with findings indicating that optimal curing conditions significantly enhance strength development [23]. Despite these important contributions, research explicitly comparing pragmatic, post-printing curing methods, such as impermeable membrane sealing, water immersion, and natural air-drying for 3DPC remains limited. This lack of data creates uncertainty for practitioners and hinders the development of robust, field-applicable best practices.

To address this gap, the present study focuses on isolating and quantifying the impact of curing on the mechanical performance of 3D-printed concrete. The primary objective is to experimentally evaluate and compare the effectiveness of three common and practical curing regimes: Natural air-drying (ND), Membrane sealing (MB), and Immersion (WI) on the development of compressive strength. Using a standardized printable mortar, this research introduces a Relative Performance Index (RPI) to provide a normalized, quantitative comparison of each method's efficacy. The findings aim to deliver a foundational, evidence-based framework for specifying effective curing protocols, thereby contributing to the reliable and widespread adoption of digital concrete construction technologies.

2. Materials and methods

2.1. Materials and Mix Proportions

In this research, materials used for mixing concrete include Ordinary Portland Cement with grade PCB40, Class F Fly Ash, natural sand, crushed sand, superplasticizer, polypropylene fiber, and water.

Ordinary Portland cement by Chiffon and fly ash (FA) by Haiphong thermal power plant, were used to form the binder component. According to ASTM C618, Hai Phong fly ash has a loss on ignition of 3.44 %, a total of SiO_2 + Al_2O_3 + Fe_2O_3 equal to 73.94 % , which is higher than 70 %, a specific gravity of 2.15 g/cm^3, and a residue on the 75 μm sieve of 6.4 %, classified as Class F [24].

The waste rock produced during coal mining that can be used as raw material for manufacturing crushed sand is sandstone. This material is most abundant in Quang Ninh province. Crushed sand with a nominal maximum aggregate size of 2.5 mm and commercially available river natural sand with a nominal maximum aggregate size of 1.5 mm were used.

Polypropylene (PP) fibres were used to decrease the shrinkage of the printed concrete. The main properties of PP fibre are listed in Table 1.

Table 1. Properties of the PP fibre.

Tensile strength	500 MPa
Modulus	6000 MPa
Diameter	35 + /-5 μm
Length	12 mm
Specific density	0.910 kg/l

To adjust the workability of the fresh concrete Superplasticizer, Viscocrete 3000-200M was used. Materials used for mixing concrete in this research are presented in Figure 1 and properties are listed in Table 2.

Figure 1. Ingredients of fiber concrete.

Table 1. Properties of binder and aggregates.

Material	Density (kg/m3)	Sieve size (mm)
Cement (Chiffon PC40)	2.98	0.08
Fly ash (Haiphong Thermal Power)	2.02	0.08
Natural sand (Lo River)	1.41	1.25
Crushed sand (Quang Ninh Province)	1.405	2.5

The mix proportions were designed based on the procedure proposed in Figure 2 and are listed in Table 3.

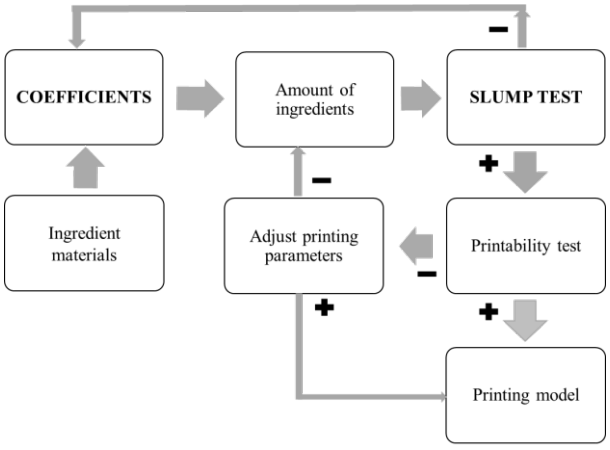

Figure 2. Mix proportion design process [25].

Table 2. Mix proportions.

Cement	Fly Ash	Water	Natural sand	Crushed sand	Fiber (%)	SP (%)
0.7	0.3	0.32	0.5 (sieve 1.25mm)	0.5 (sieve 2.5mm)	0.25	0.4

(Note: Binder = Cement and Fly Ash; values in Table are ratios of each ingredient to binder weight)

2.2. Printing task

The digital fabrication workflow commenced with the creation of a 3D model, exported in the standard ".STL" format. This model was processed using Simplify3D software [26] for slicing, where key parameters, including a 10 mm layer height, were defined to generate the machine instructions (".Gcode"). The G-code was subsequently executed by a custom-built 3D concrete printer, controlled via Mach3 software [27], which coordinated the motion system. A 22 mm diameter round nozzle was used for material deposition. This integrated software pipeline, illustrated in Figure 3, ensured precise layer-by-layer fabrication of the designed geometry.

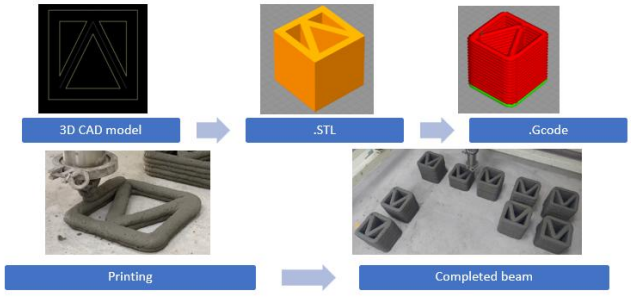

Figure 3. Steps of the printing process.

2.3. Curing Regimes

After being printed for 24 hours, specimens were assigned to one of three curing regimes for the duration until testing, as shown in Figure 4:

Water Immersion (WI): Specimens were fully immersed in a lime-saturated water tank. This moist curing method complies with ASTM C31/C31M [28] and the principles of TCVN 8828:2011[20], using water meeting TCVN 4506:2012 [29] requirements.

Membrane Curing (MB): Specimens were sealed with three layers of polyethylene film to prevent evaporation. This method aligns with impermeable sheeting practices in ASTM C171 and the waterproof covering method specified in TCVN 8828:2011.

Natural Air-Drying (ND): Specimens were exposed to uncontrolled laboratory air and watered water everyday, representing a baseline condition without moisture control, following general specimen conditioning principles.

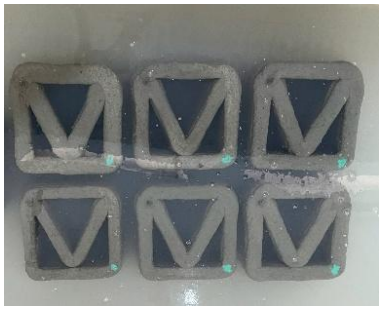

(a) Water Immersion

(b) Membrane Sealing

(c) Natural air-drying

Figure 4. Curing methods for 3D-printed concrete samples.

2.4. Testing Procedure

The compressive strength of all specimens was determined through uniaxial compression tests performed at the target ages of 7 and 28 days. Testing was conducted using a servo-hydraulic universal testing machine with a load capacity of 2000 kN, as shown in Figure 5.

Figure 5. Compression test of 3D-printed concrete samples.

The test procedure was designed to ensure consistency and compliance with the standardized method outlined in TCVN 3118:1993 (Heavyweight concrete – Method for determination of compressive strength) [30].

Specimen Preparation and Mounting: Before testing, the top and bottom surfaces of each specimen were checked for evenness. Specimens were centered on the lower bearing plate of the testing machine. A spherical seating was used on the upper platen to ensure uniform load distribution and minimize eccentricity.

Loading Protocol: A monotonic, displacement-controlled loading regime was applied. The load was increased continuously at a constant rate of 0.5 MPa per second until specimen failure, as prescribed by the standard. This controlled rate prevents sudden shock loading and allows for consistent measurement of the peak load.

Data Acquisition and Measurement: The machine's integrated load cell and displacement transducer recorded the applied load and platen displacement throughout the test. The maximum load P at failure, in Newtons (N), was recorded for each specimen. The compressive strength f_c was calculated using the (Eq.1):

$$f_c = \frac{P}{A} \quad (Eq.1)$$

The contact area, denoted as A, refers to the surface area of the compression platen in direct contact with the specimen during testing, measured in mm^2. For the printed specimens in this study, area A was derived from their designed geometry: a 200 mm x 200 mm boundary frame with an internal triangular rib of 310 mm in length. Assuming an average filament deposition width of 30 mm, the total calculated contact area was 33,300 mm^2. This value was consequently adopted for A in all subsequent calculations.

Replication and Testing Matrix: To ensure statistical reliability, three replicate specimens were tested for each unique condition (i.e., for each curing method at each testing age). This resulted in a total of 18 compressive strength tests (3 curing methods × 2 testing ages × 3 replicates).

Cracking patterns Documentation: Following each test, the characteristic cracking patterns of the specimen were visually documented through photography. This qualitative analysis was crucial for correlating strength performance with observed fracture patterns, particularly to identify interlayer delamination in printed specimens.

3. Results and discussion

3.1. Compressive Strength Results

The compressive strength results of 3D-printed concrete specimens under three different curing regimes at 7 and 28 days are presented in Table 4 and Figure 6. The average values and standard deviations were calculated from three replicates per condition.

Table 3. Compressive strength of 3D-printed concrete under different curing methods.

Curing Method	Specimen	7-Day Strength (MPa)	28-Day Strength (MPa)
Natural Air-drying (ND)	ND 1	9.3	15.8
	ND 2	11.3	16.6
	ND 3	11.6	15.0
Average ± SD		10.7 ± 1.2	15.8 ± 0.8
Membrane (MB)	MB 1	16.0	19.0
	MB 2	18.2	21.6
	MB 3	16.0	18.4
Average ± SD		16.7 ± 1.3	19.7 ± 1.6
Water Immersion (WI)	WI 1	14.5	17.2
	WI 2	11.7	17.5
	WI 3	13.2	17.8
Average ± SD		13.1 ± 1.4	17.5 ± 0.3

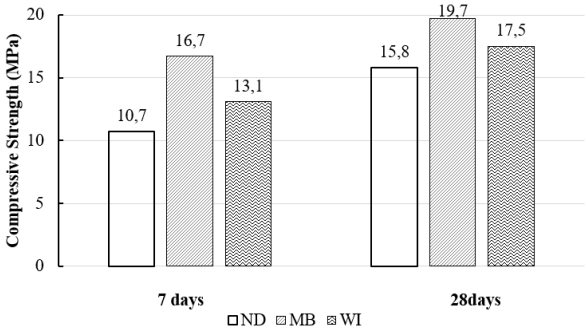

Figure 6. Compressive strength of 3D-printed concrete under different curing methods.

3.2. Effect of Curing Method on Strength Development

The data clearly indicate that the curing method significantly influences the compressive strength development of 3D-printed concrete.

At 7 days, the highest average strength was achieved by the Membrane (MB) curing method (16.7 MPa), followed by Immersion (WI) curing (13.1 MPa), and lastly Natural (ND) curing (10.7 MPa). This suggests that early-age strength is highly sensitive to moisture retention, with Membrane curing providing the most effective barrier against evaporation.

At 28 days, the same ranking is observed: MB (19.7 MPa) > WI (17.5 MPa) > ND (15.8 MPa). The superior performance of Membrane curing is maintained, indicating its effectiveness not only in early strength gain but also in long-term strength development.

An interesting observation is that Immersion (WI) curing did not yield the highest strength, contrary to common expectations for traditional concrete. This could be attributed to the specific porosity and layered microstructure of 3D-printed concrete, where continuous immersion might not be as beneficial as preventing moisture loss through sealing. Natural air-drying resulted in the lowest strength, highlighting the critical need for active moisture control in 3DCP.

To quantitatively compare the effectiveness of each curing method relative to the best-performing one, a *Relative Performance Index (RPI)* was calculated. The Membrane (MB) curing method was used as the baseline (100 %) for this index, as it consistently yielded the highest average compressive strength at both ages. The RPI for each group was calculated using the (Eq.2):

$$\mathrm{RPI}_{\mathrm{group}}(\%) = \left(\frac{f_{c,group}}{f_{c,MB}}\right) \times 100 \quad (Eq.2)$$

Where:

$\bar{f}_{c,\,\mathrm{group}}$ is the average compressive strength of a given curing method (ND, MB, or WI).

$\bar{f}_{c,\,\mathrm{MB}}$ is the average compressive strength of the Membrane (MB) curing method.

The calculated RPI values for all methods at 7 and 28 days are summarized in Table 5.

The RPI provides a clear, normalized measure of performance retention. The results indicate that:

- At 7 days, the Immersion (WI) method retained approximately 78 % of the performance achieved by the optimal Membrane curing. The Natural (ND) method retained only about 64 %, revealing a substantial early-age deficit due to moisture loss.

- At 28 days, the performance gap narrowed but remained significant. The Immersion method improved to retain nearly 89 % of the baseline strength, while the Natural method reached about 80 %.

This trend underscores two critical points:

- The Superior Efficacy of Membrane Curing: Its ability to completely prevent moisture evaporation resulted in the highest strength development, establishing it as the most effective method under the tested conditions.

- The Heightened Vulnerability at Early Ages: The larger performance gap at 7 days compared to 28 days highlights that improper curing immediately after printing has a more severe impact on early strength gain. This is particularly crucial for 3D-printed concrete, where early-age properties influence interlayer bonding and structural build-up during the printing process itself.

The results strongly support the use of Membrane (sealing) curing as a highly effective and practical method for 3D-printed concrete in construction. It outperformed both Immersion and Natural air-drying in this study, likely due to its ability to effectively lock in mixing water without the potential drawbacks of immersion (e.g., water saturation, leaching) or the risks of natural drying. This method is also more feasible for on-site application compared to continuous immersion.

Table 4. Relative Performance Index (RPI) of the curing methods.

Curing Method	Average Strength, 7-day (MPa)	RPI at 7 days (%)	Average Strength, 28-day (MPa)	RPI at 28 days (%)
Membrane (MB)	16.7	100	19.7	100
Immersion (WI)	13.1	78.4	17.5	88.8
Natural (ND)	10.7	64.1	15.8	80.2

3.3. Cracking patterns

In conjunction with the quantitative strength measurements, the macroscopic failure modes of all tested specimens were documented to provide qualitative insight into the mechanical behavior and the influence of curing on failure mechanisms. Following each compressive test, the fracture pattern was visually inspected and recorded.

Across all curing methods and at both testing ages, the dominant and consistent cracking patterns observed were predominantly vertical cracking, as shown in Figure 7, leading to a classical columnar crushing failure. This pattern indicates that under uniaxial compression, the printed elements behaved in a relatively cohesive and monolithic manner, with the applied stress being redistributed through the bulk material matrix rather than being predominantly dissipated along the interlayer interfaces.

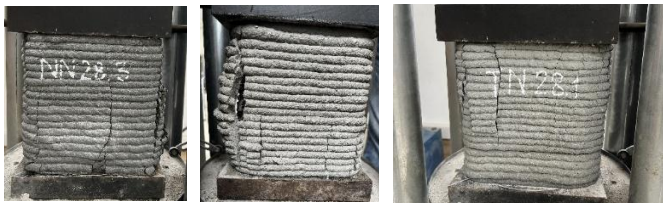

Figure 7. Vertical cracking failure in 3D-printed concrete.

Isolated instances of inclined cracking were observed in a few non-typical specimens, but the angle of these cracks was notably shallow, as shown in Figure 8. Crucially, no distinct delamination or lateral splitting along the printed layer interfaces was observed in any of the 18 tested specimens.

Figure 8. Inclined cracking failure in 3D-printed concrete.

This qualitative observation of cracking patterns is significant, as shown in Figure 9. It suggests that, for the specific material composition and printing parameters used in this study, the interlayer bonds, though potentially affected by curing as reflected in the strength measurements, were sufficiently robust to prevent adhesive failure. The consistent vertical cracking patterns support the interpretation that the measured strength differences between curing regimes are attributable to variations in the generalized material strength and matrix quality rather than to a complete, localized failure of the interlayer bonds. This finding underscores that proper curing enhances the overall homogeneity and integrity of the printed microstructure.

Figure 9. Cracking patterns of 3D-printed concrete samples.

4. Conclusion

This study systematically evaluated the effects of three practical curing methods, including Membrane sealing (MB), Water Immersion (WI), and Natural air-drying (ND), on the compressive strength development of 3D-printed concrete. The key findings demonstrate that the curing method has a statistically significant impact on mechanical performance. Membrane curing emerged as the most effective method, yielding the highest compressive strength at both 7 days (16.7 MPa) and 28 days (19.7 MPa). This superior performance is attributed to its ability to completely prevent moisture evaporation, which is critical for the hydration of the high-surface-area, layered microstructure of printed concrete.

While Immersion curing provided better moisture retention than natural exposure, it was less effective than membrane sealing, achieving only 89 % of the 28-day baseline strength. This indicates that for 3D-printed concrete, an effective moisture barrier is more crucial than continuous water contact.

Natural air-drying resulted in the poorest performance, with a significant relative performance deficit of 20 % at 28 days and 36 % at 7 days. This severe strength reduction, corroborated by observed interlayer delamination failures, underscores the critical vulnerability of 3D-printed concrete to uncontrolled drying and highlights the necessity of proactive moisture control.

The introduced Relative Performance Index (RPI) successfully quantified these performance differences, providing a clear, normalized metric for comparing curing efficacy. From a practical standpoint, these findings strongly recommend impermeable membrane curing as a vital, on-site best practice to ensure the structural integrity and reliable performance of 3D-printed concrete elements.

Qualitative analysis of cracking patterns revealed cohesive vertical cracking without interlayer delamination across all specimens. This indicates that the interlayer bonds were competent, and the strength reduction under poor curing is primarily due to a generalized weakening of the bulk matrix rather than isolated bond failure. This finding reinforces the importance of proper curing in achieving homogeneous material quality in 3D-printed concrete.

Acknowledgements

The authors acknowledge the financial support from the STSC research group, the material provision from Thanh Hung Concrete Joint Venture Company, and the laboratory support from Haiphong University, Vietnam.

Referrences

[1]. M. Surya, S. K. Singh, and S. K. Kirthika, “3-D Printing in Construction: A Review,” Nbm&Cw. 2019. [Online]. Available: https://www.nbmcw.com/report/construction-infra-industry/39828-3-d-printing-in-construction-a-review.html

[2]. Blogin3D, “Công Nghê In 3D Bê Tông: Kỷ Nguyên Xây Nhà Với Máy In 3D.” [Online]. Available: https://blogin3d.com/cong-nghe-in-3d-be-tong-ky-nguyen-xay-nha-voi-may-in-3d.html

[3]. L. Minh, “Công nghệ in 3D trong xây dựng,” Bộ Xây dựng. [Online]. Available: http://moc.gov.vn/vn/tin-tuc/1145/52213/cong-nghe-in-3d-trong-xay-dung.aspx

[4]. S. Cho, J. Kruger, S. Zeranka, and G. Van Zijl, “3D Printable Concrete Technology and Mechanics,” vol. 158, no. September, pp. 11–18, 2019.

[5]. H. Tu, Z. Wei, A. Bahrami, N. Ben Kahla, A. Ahmad, and Y. O. Özkılıç, “Recent advancements and future trends in 3D concrete printing using waste materials,” Dev. Built Environ., vol. 16, no. April, 2023, doi: 10.1016/j.dibe.2023.100187.

[6]. T. Wangler et al., “Digital Concrete: Opportunities and Challenges,” RILEM Tech. Lett., vol. 1, p. 67, Oct. 2016, doi: 10.21809/rilemtechlett.2016.16.

[7]. A. K. Al-Tamimi, H. H. Alqamish, A. Khaldoune, H. Alhaidary, and K. Shirvanimoghaddam, “Framework of 3D Concrete Printing Potential and Challenges,” Buildings, vol. 13, no. 3, 2023, doi: 10.3390/buildings13030827.

[8]. I. Kothman and N. Faber, “How 3D printing technology changes the rules of the game Insights from the construction sector,” J. Manuf. Technol. Manag., vol. 27, no. 7, pp. 932–943, 2016, doi: 10.1108/JMTM-01-2016-0010.

[9]. X. Lyu et al., “Mechanical performance and anisotropic analysis of rubberised 3D-printed concrete incorporating PP fibre,” Environ. Sci. Pollut. Res., vol. 31, no. 36, pp. 49100–49115, Jul. 2024, doi: 10.1007/s11356-024-34437-w.

[10]. B. Panda, S. Chandra Paul, and M. Jen Tan, “Anisotropic mechanical performance of 3D printed fiber reinforced sustainable construction material,” Mater. Lett., vol. 209, pp. 146–149, Dec. 2017, doi: 10.1016/j.matlet.2017.07.123.

[11]. K. Liu, K. Takasu, J. Jiang, K. Zu, and W. Gao, “Mechanical properties of 3D printed concrete components: A review,” Dev. Built Environ., vol. 16, no. August, p. 100292, 2023, doi: 10.1016/j.dibe.2023.100292.

[12]. B. Panda, N. A. N. Mohamed, S. C. Paul, G. V. P. B. Singh, M. J. Tan, and B. Šavija, “The effect of material fresh properties and process parameters on buildability and interlayer adhesion of 3D printed concrete,” Materials (Basel)., vol. 12, no. 13, 2019, doi: 10.3390/ma12132149.

[13]. R. J. M. Wolfs, F. P. Bos, and T. A. M. Salet, “Hardened properties of 3D printed concrete: The influence of process parameters on interlayer adhesion,” Cem. Concr. Res., vol. 119, no. January, pp. 132–140, 2019, doi: 10.1016/j.cemconres.2019.02.017.

[14]. B. Nan, Y. Qiao, J. Leng, and Y. Bai, “Advancing Structural Reinforcement in 3D-Printed Concrete: Current Methods, Challenges, and Innovations,” Materials (Basel)., vol. 18, no. 2, 2025, doi: 10.3390/ma18020252.

[15]. B. Panda, S. C. Paul, N. A. N. Mohamed, Y. W. D. Tay, and M. J. Tan, “Measurement of tensile bond strength of 3D printed geopolymer mortar,” Measurement, vol. 113, pp. 108–116, Jan. 2018, doi: 10.1016/j.measurement.2017.08.051.

[16]. B. Panda and M. J. Tan, “Experimental study on mix proportion and fresh properties of fly ash based geopolymer for 3D concrete printing,” Ceram. Int., vol. 44, no. 9, pp. 10258–10265, 2018, doi: 10.1016/j.ceramint.2018.03.031.

[17]. K. Yu, W. McGee, T. Y. Ng, H. Zhu, and V. C. Li, “3D-printable engineered cementitious composites (3DP-ECC): Fresh and hardened properties,” Cem. Concr. Res., vol. 143, p. 106388, May 2021, doi: 10.1016/j.cemconres.2021.106388.

[18]. K. Yu, W. McGee, T. Y. Ng, H. Zhu, and V. C. Li, “3D-printable engineered cementitious composites (3DP-ECC): Fresh and hardened properties,” Cem. Concr. Res., vol. 143, no. May 2020, p. 106388, 2021, doi: 10.1016/j.cemconres.2021.106388.

[19]. “ACI 308R-18 Guide to Curing Concrete.” American Concrete Institute (ACI), Farmington Hills, MI, USA, 2018. [Online]. Available: https://www.concrete.org/store/productdetail.aspx?ItemID＝308R18

[20]. “TCVN 8828:2011 Concrete-Requirements for natural moist curing.” Bộ Khoa học và Công nghệ, 2011.

[21]. M. Nodehi, T. Ozbakkaloglu, and A. Gholampour, “Effect of supplementary cementitious materials on properties of 3D printed conventional and alkali-activated concrete: A review,” Autom. Constr., vol. 138, p. 104215, Jun. 2022, doi: 10.1016/j.autcon.2022.104215.

[22]. Y. Chen, Z. Chang, S. He, O. Çopuroğlu, B. Šavija, and E. Schlangen, “Effect of curing methods during a long time gap between two printing sessions on the interlayer bonding of 3D printed cementitious materials,” Constr. Build. Mater., vol. 332, p. 127394, May 2022, doi: 10.1016/j.conbuildmat.2022.127394.

[23]. Y. Wei and H. Zhang, “Influence of Temperature and Humidity on Mechanical Properties of Calcined Oyster-Shell Powder-Modified 3D-Printed Concrete,” ACS Omega, vol. 9, no. 37, pp. 39180–39187, Sep. 2024, doi: 10.1021/acsomega.4c06129.

[24]. P. T. Duc, “Research on using original fly ash of Hai Phong thermal power plant as a mineral additive to improve the properties of large concrete blocks,” Hai Phong, 2019.

[25]. L. T. Pham et al., “Development of 3D printers for concrete structures: mix proportion design approach and laboratory testing,” Smart Sustain. Built Environ., vol. 12, no. 5, pp. 1056–1073, Nov. 2023, doi: 10.1108/SASBE-07-2022-0137.

[26]. “Simplify3D Desktop Software.” [Online]. Available: https://www.simplify3d.com/

[27]. G. University, “Mach3 CNC Control Software.” [Online]. Available: https://www.goodwin.edu/glossary/mach-3-cnc-control-software

[28]. “ASTM C31/C31M-21 - Standard Practice for Making and Curing Concrete Test Specimens in the Field.” ASTM International, West Conshohocken, PA, 2023.

[29]. “TCVN 4506:2012 Water for concrete and mortar – Technical requirements.” Ministry of Science and Technology, Hanoi, 2012.

[30]. TCVN 3118:1993, “Bê tông nặng – Phương pháp xác định cường độ nén (Heavyweight concrete - Method for determinatien of compressive strength),” Bộ Xây dựng. pp. 2–6, 1993.